

Study of the Effects of the Magnetic Field on the Anodic Dissolution of Nickel With In-Line Digital Holography

Ming Zhang¹, Boyu Yuan¹, Qiong Wu¹, Yongyan Zhu¹, Liang Li^{1,*}, Chao Wang^{1,2,*}

¹ Jiangsu Key Laboratory of Green Synthetic Chemistry for Functional Materials, School of Chemistry & Chemical Engineering, Jiangsu Normal University, Xuzhou 221116, China

² Xuzhou Institute of Technology, Xuzhou 221111, China

*E-mail: lil@jsnu.edu.cn(Liang Li), wangc@jsnu.edu.cn(Chao Wang).

Received: 12 September 2017 / Accepted: 11 November 2017 / Published: 16 December 2017

Anodic dissolution of nickel in HNO₃+Cl⁻ solutions was studied with in-line digital holography by observing the dynamic processes at the electrode-electrolyte interface under an applied magnetic field. Although the Lorentz force always enhances the mass-transport processes, the effects of the magnetic field on the anodic dissolution of nickel have been found to be different in different regions. In the active region, because electron transfer rather than mass transfer is the rate-determining step, the magnetic field decreases the current, as confirmed by the decrease in the concentration gradient of the corrosion products at the interface. The convection induced by the magnetic field drives away intermediate ions such as Ni(CIH⁺)_{ads} from the surface of the electrode, which can inhibit the formation of the surface film. However, in the prepassive region, since mass transfer is the rate-determining step, the current increases, and the concentration gradient of the corrosion products increases at the interface.

Keywords: Nickel; Anodic dissolution; Magnetic field; Digital holography

1. INTRODUCTION

Magnetochemistry, as a branch of electrochemistry, has been studied since the 1930s owing to its practical applications in industry. Recently, interest in magnetochemistry has mainly been directed at the effects of the magnetic field (MF) on mass transport [1-6], electrode kinetics [7-10], and deposit morphology [11-15].

It is well-established that an MF can modify the mass transport rate by the magnetohydrodynamic (MHD) effect [4,16-19]. The origin of the effect is the Lorentz force (F_L) that generates the convection of the solution to increase the limiting current [16]. Unlike the high degree of agreement on the mass transport processes, the effects of MF on electron-transfer processes are

controversial. Olivier [7] studied different electrochemical systems by electrochemical impedance spectroscopy and proposed that MF has no effect on the charge-transfer coefficient. Koehler [8] failed to detect any changes induced by MF for the electron-transfer rate constant of different redox couples. However, Lu [20] and Li [21] reported that MF does affect the electron-transfer step directly or indirectly.

Both traditional and modern techniques, such as the voltammetric technique [22], electrochemical impedance spectroscopy (EIS) [2] and scanning tunnelling microscopy (STM) [23], have been applied to investigate the effect of MF on the anodic dissolution of metallic materials and have made fruitful contributions. However, to date, in-line techniques have been rarely used in the studies of the effects of MF on the anodic dissolution of the nickel electrode. In-line digital holography, a newly developed technique in the field has been found to show several advantages in the study of the dynamic processes of the electrochemical reactions at the electrode-electrolyte interface [24-25], namely, real time dynamics, fast response, high precision, and the non-destructive working principle [26].

Compared with the large number of papers on the effects of MF on the anodic dissolution of iron [27-33] and copper [4,6,34-39], there have been relatively few studies concerning MF effects on the anodic dissolution of nickel [40]. Our previous study [21] found that an applied MF promoted the anodic dissolution when a mass-transfer process was the rate-determining step. However, when the electron-transfer process was the rate-limiting step, the MF effects became complicated. Thus, more information is needed to explain how MF affects the electron-transfer step.

2. EXPERIMENTAL

The electrochemical experiments were carried out in a traditional three-electrode cell consisting of a nickel working electrode (99.98%, Johnson Matthey Company), a Pt sheet counter electrode and a saturated calomel electrode (SCE) as the reference electrode. The working electrode (diameter and length of 2 mm and 20 mm, respectively) was sealed with a layer of epoxy resin placed in a glass tube with one end tightly welded to a Cu wire and the other end exposed to the solutions. Prior to each experiment, the exposed end was polished with emery papers and then washed with doubly distilled water in an ultrasonic bath. The IR drop was minimized by employing a Luggin capillary between the working and the reference electrodes. Unless indicated otherwise, the solution used in this study was 0.5 M HNO₃ + 2.0 mM NaCl prepared from analytical grade reagents and doubly distilled water. All potentials in this study are in reference to SCE.

The cell was placed in the gap of two ferromagnets, which induced a homogeneous field of up to 0.45 T parallel to the surface of the electrode. The in-line digital holography experimental setup is described in [41].

Figure 1 shows a schematic diagram of the digital holography setup. The beam generated by a He-Ne laser (wavelength: 632.8 nm) was separated into two by a beam splitter (BS). Neutral Density Filters (NDF) were used to adjust the reference wave to maintain its intensity the same as that of the object wave. The concentration changes near the surface of the electrode were detected via the beams and then recorded as holograms by a CCD camera (Sony, DSR-PD150P), which was connected to a

computer. In the presence of a concentration change (Δc) near the surface of the electrode during the anodic dissolution processes of nickel, a phase difference ($\Delta\Phi$) and refractive index variation (Δn) were observed. The relationships between $\Delta\Phi$, Δc , and Δn are described by [35]:

$$\Delta c = k\Delta n = k\lambda_0\Delta\Phi / (2\pi d) \quad (1)$$

where k is the concentrative refractivity, λ_0 is the laser light wavelength and d is the geometrical path length where the refractive index variation is present.

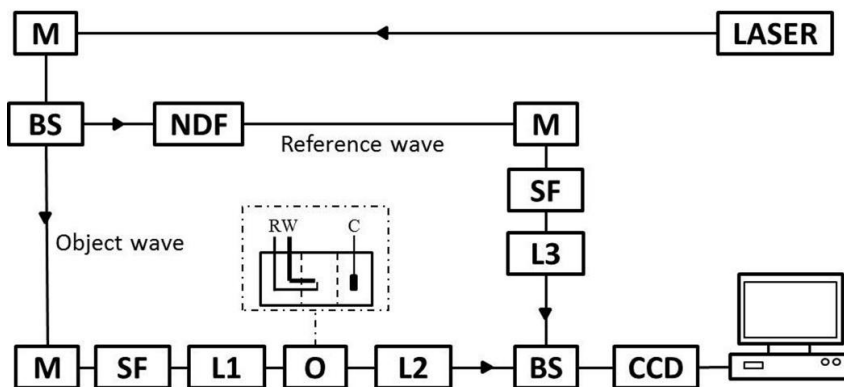


Figure 1. Schematic diagram of the holographic system. M: mirror; BS: beam splitter; NDF: Neutral Density Filters; SF: spatial filter; O: experimental cell; L1, L2 and L3: lens.

The surface morphology of nickel was observed by scanning electron microscopy (Hitachi S-3400N). The electrochemical experiments were carried out by a CHI604B electrochemical instrument. The potentiodynamic polarization (scan rate of 10 mV/s) and chronoamperometry methods were used. All experiments were conducted at room temperature ($25 \pm 2^\circ\text{C}$).

3. RESULTS AND DISCUSSIONS

3.1 Anodic polarization curves

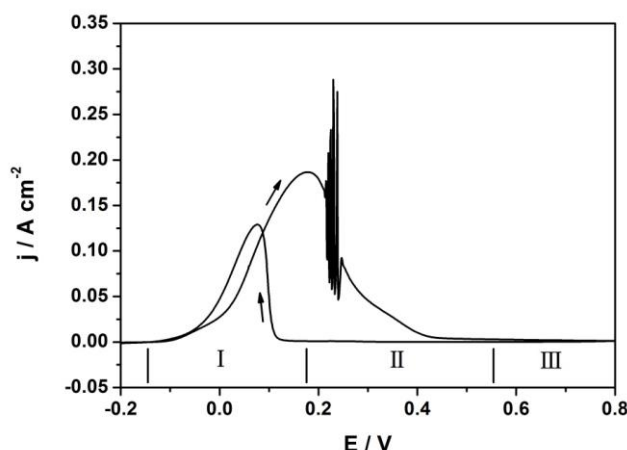


Figure 2. The polarization curve of the Ni | 0.50 M HNO₃ + 2.0 mM NaCl system without MF; scan rate: 10 mV / s.

Figure 2 shows the anodic polarization curve of the Ni electrode in 0.5 M HNO₃ + 2.0 mM NaCl solution without MF with the scan rate of 10 mV/s. As in the 0.5 M HNO₃ + 5.0 mM NaCl solution, the overall anodic process can be roughly divided into three regions [21]. In the active region (I), the current increases with the increase of the potential until a peak appears; in the prepassive region (II), the current decreases with the increase of the potential because the formation rate of the surface film tends to exceed the dissolution rate; in the passive region (III), a passive film is formed on the surface of the electrode with defects due to chloride ions.

3.2 Effects of MF on the *j-t* curves

3.2.1 In the active region

Figure 3 shows the *j-t* curves at 0.04 V in the active region (I) without and with the application of MF. Examination of Figure 3 shows that MF decreases the current. In our previous paper [21], it was proposed that the applied MF drove the intermediate ions (such as NiClH⁺) inhibiting the formation of the surface film away from the surface of the electrode so that the active dissolution was inhibited. For further study, in-line digital holography was used to observe the dynamic processes at the electrode-electrolyte interface during the active dissolution.

Figure 4 shows the distribution of the holograms at different time points corresponding to Figure 3. The phase difference is caused by the change of the refractive index, which is linked to the changes of the concentration of the substances at the interface. The left side is the electrode while the right side is the electrolyte (Figure 4). The green area means the phase difference is almost zero, indicating that the concentration is uniform, whereas the red and the yellow areas reflect the increase of the phase difference, indicating the increase of the concentration of the corrosion products at the interface. Figures 4a and 4a' show the phase distribution before polarization without (Figure 4a) or with (Figure 4a') the application of MF. The entire areas being solely green indicates that the concentration is constant at the interface. Without the MF application (Figures 4b-4e), yellow and red areas are observed at the interface, indicating that the concentration of the corrosion products increases obviously with time. The values of the phase changes in the absence of MF (Figures 4b-4e) are larger than those in the presence of MF (Figures 4b'-4e'), indicating that the concentration of the corrosion products with the application of MF is lower than that without the application of MF.

There are different opinions regarding the effects of MF on the charge-transfer step. Lu [31] proposed that MF hardly affected the activation-controlled anodic current of iron in the NaHCO₃ solutions without halides, and Sueptitz [42] also proposed that the effects of MF on the current density were not obvious in the active region for the iron electrode in the phthalate buffer. It is generally accepted that in highly concentrated electrolytes, there was no impact of MF on the anodic dissolution of iron controlled by the charge transfer step [27,43-46].

However, in the relatively low concentration electrolytes, for example, during the anodic dissolution of iron in dilute H₂SO₄ in the potential region controlled by the charge transfer step [33], it has been proposed that the anodic current is slightly decreased by MF because F_L drives the Fe²⁺-ions away and the H⁺-ions towards the electrode surface. While an applied MF affects the anodic

dissolution [33], F_L does not affect the charge transfer step directly but may affect the ion concentrations near the surface of the electrode.

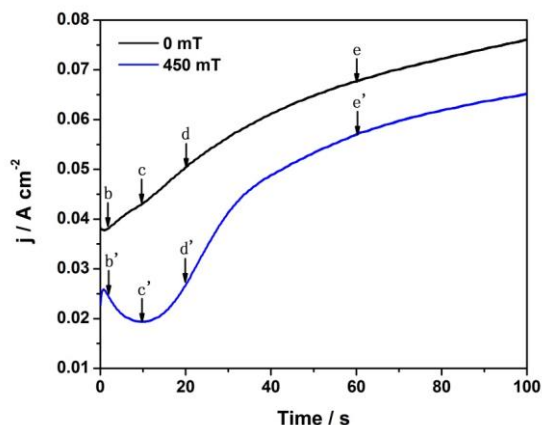


Figure 3. The j - t curves of Ni in 0.5 M HNO_3 + 2.0 mM Cl^- solutions without and with MF at $E = 0.04$ V.

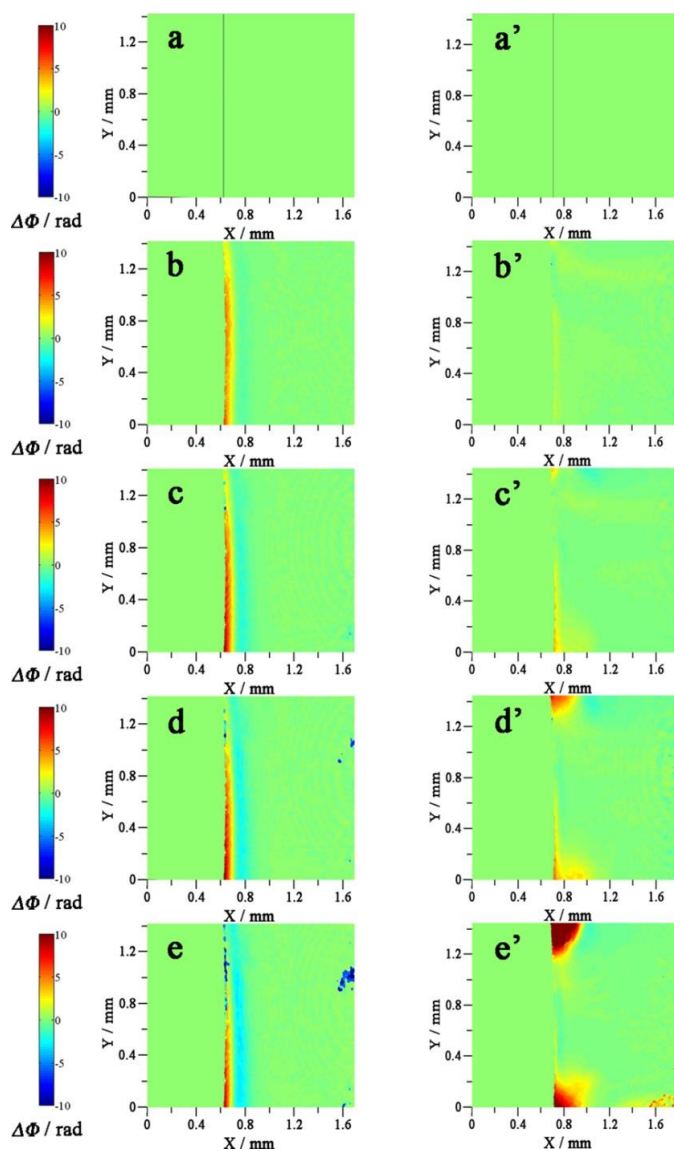


Figure 4. Phase distributions at different times corresponding to Figure 2 without (b-e) and with MF parallel (b'-e'). a, a': the phase distribution before the test without (a) or with MF (a').

For the study of the MF effects, the possible reactions during the anodic dissolution of the Ni electrode in an acidic solution containing chloride ions are given as follows [47]:



Darwish *et al.* [48] proposed a similar mechanism for the dissolution of iron in acidic chloride solutions. Haleem [47] proposed that the rate-determining step was Reaction (2). The intermediate ions, such as $\text{Ni}(\text{ClH}^+)_{\text{ads}}$, can promote reaction (3), and it may occur on the surface of the electrode at the initial stage of the active dissolution. After MF is applied, F_L is induced to force this type of ion to leave the surface of the electrode (Figures 4b'-4e'), thus inhibiting reaction (3). As a consequence, the current (Figure 3) and the concentration of the corrosion products (such as Ni^{2+}) decrease with the application of MF (Figure 4).

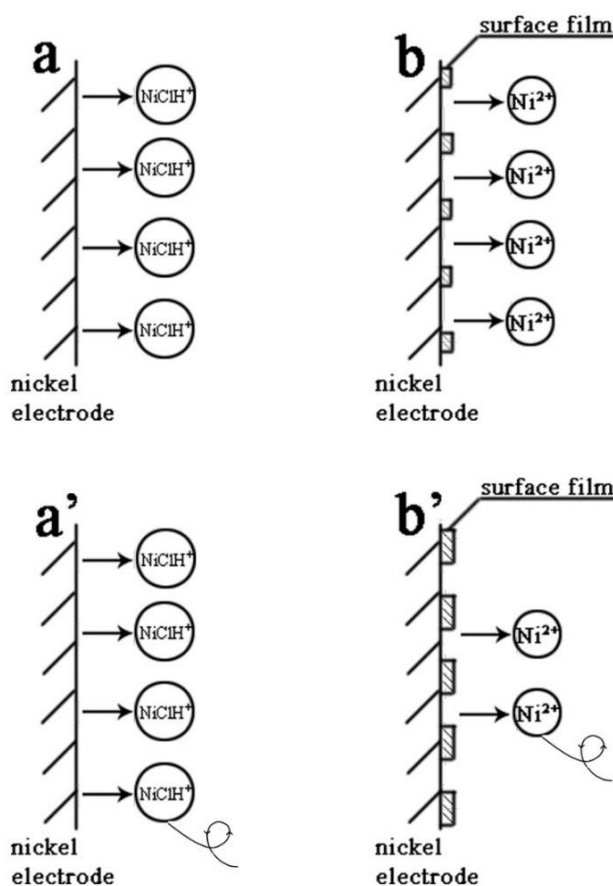


Figure 5. Schematic plot of anodic dissolution of nickel in the active region without (a and b) and with (a' and b') MF.

Figure 5 illustrates the anodic dissolution of nickel in the active region without (a and b) and with (a' and b') MF. Without MF application (Figures 5a-5b), many intermediate ions such as $\text{Ni}(\text{ClH}^+)_{\text{ads}}$ are generated on the electrode surface by reaction (2) in the primary stages of the active dissolution. Subsequently, intermediate ions such as $\text{Ni}(\text{ClH}^+)_{\text{ads}}$, are oxidized to Ni^{2+} through reaction (3), and a surface film is formed on the electrode surface. However, with the application of MF (Figures 5a'-5b'), F_L is induced to drive $\text{Ni}(\text{ClH}^+)_{\text{ads}}$ away from the electrode surface, which can inhibit

the formation of the surface film, leading to easier formation of the surface film. Even though MF increases the mass transport, electron transfer is the rate-determining step in the active region. The enhancement of mass transport caused by MF not only fails to promote the anodic dissolution but also inhibits it by accelerating the evacuation of the intermediate ions from the electrode surface.

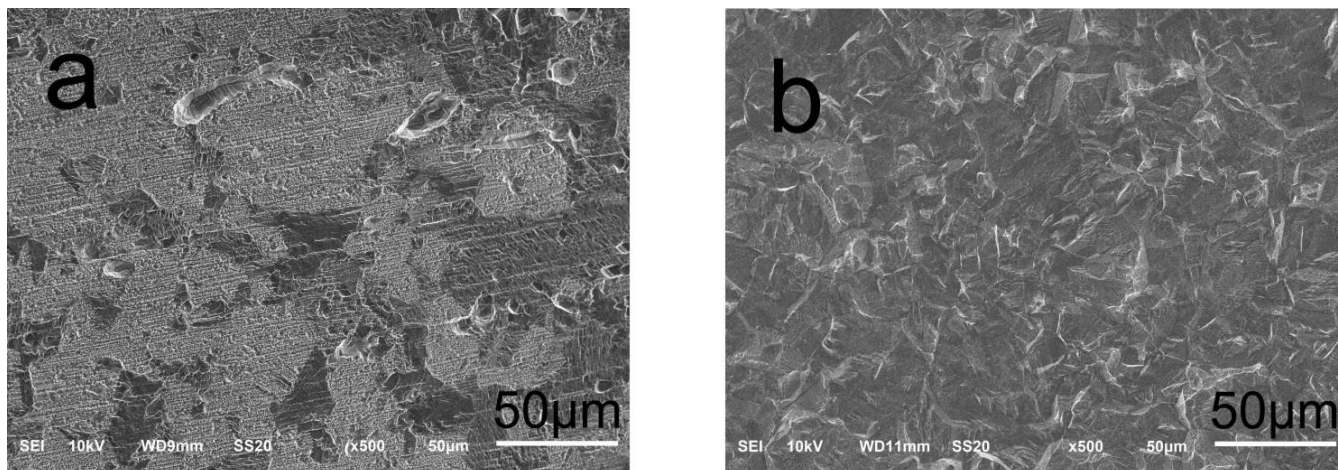


Figure 6. Surface morphologies of the electrodes in 0.5 M HNO_3 + 2.0 mM Cl^- solutions polarized at 0.04 V for 100 s without (a) and with (b) MF.

Figure 6 shows the surface morphologies of the Ni electrodes potentiostatically polarized at 0.04 V for 100 s in 0.5 M HNO_3 + 2.0 mM Cl^- solutions without and with the application of MF, respectively. In the presence of chloride ions, the surface film is formed with defects, so that pitting is easily induced. Several pits are observed on the surface of the electrode without the application of MF (Figure 6a); however, with the application of MF (Figure 6b), the surface becomes smoother than that without the application of MF. Clearly, MF inhibits the active dissolution of nickel. The results obtained by SEM, digital holography (Figure 4), and potentiostatic polarization (Figure 3) are in agreement.

In the active region, electron transfer is the rate-determining step. The intermediates are forced away from the surface of the electrode leading to the decrease of the current. What will occur under the application of MF when mass transfer is the rate-determining step? To answer this question, dynamic processes have been observed by in-line digital holography during the anodic dissolution of nickel in the prepassive region.

3.2.2 In the prepassive region

Figure 7 shows the j - t curves at 0.25 V in the prepassive region without or with the application of MF. In contrast to Figure 3, MF increases the current (Figure 7).

Figure 8 shows the distribution of the holograms at different time points corresponding to Figure 7. Figures 8a and 8a' show the phase distribution before polarization without (Figure 8a) and with (Figure 8a') the application of MF, respectively. As shown in Figures 8b-8e, relatively uniform

yellow and red areas are observed at the interface without the application of MF; however, these areas retreat to the edges of the electrode (Figures 8b'-8e') with the application of MF.

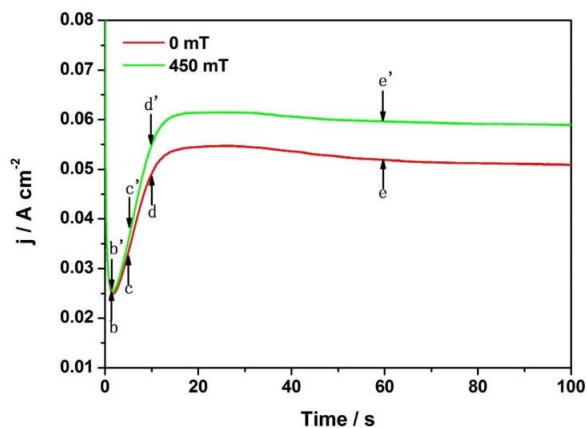


Figure 7. The j - t curves of Ni in 0.5 M HNO_3 + 2.0 mM Cl^- solutions without and with MF at $E= 0.25$ V.

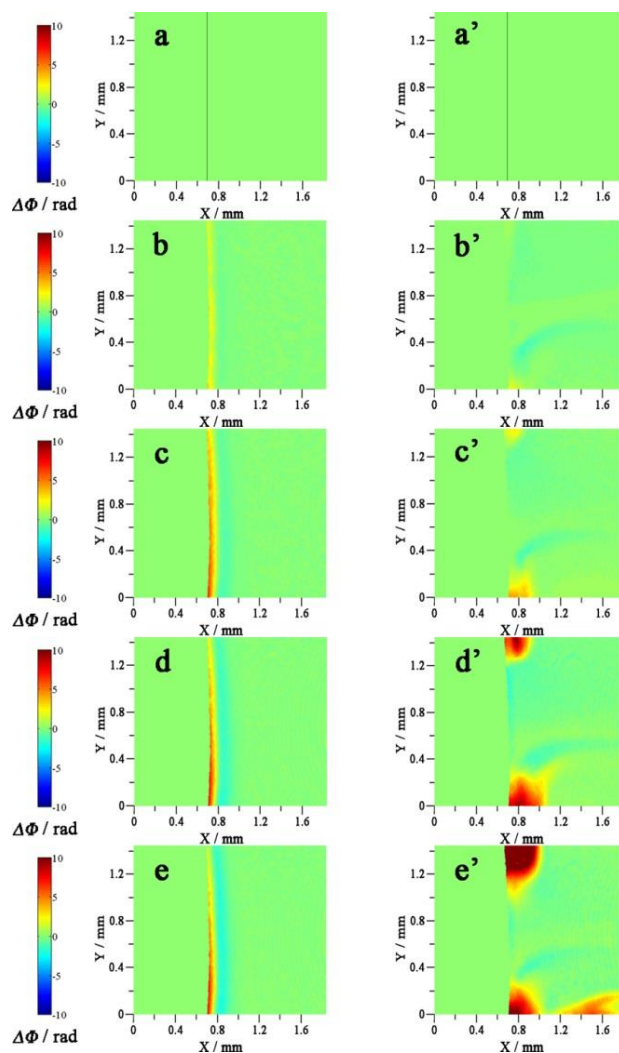


Figure 8. Phase distributions at different times corresponding to Figure 6 without (b-e) and with MF parallel (b'-e'). a, a': the phase distribution before the test without (a) or with MF (a').

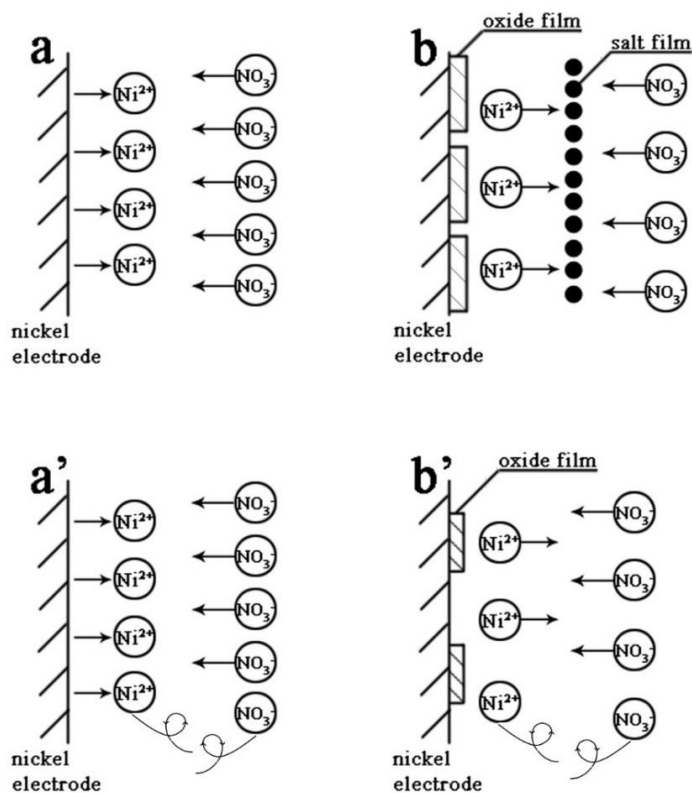


Figure 9. Schematic plot of anodic dissolution of nickel in the prepassive region without (a and b) and with (a' and b') MF.

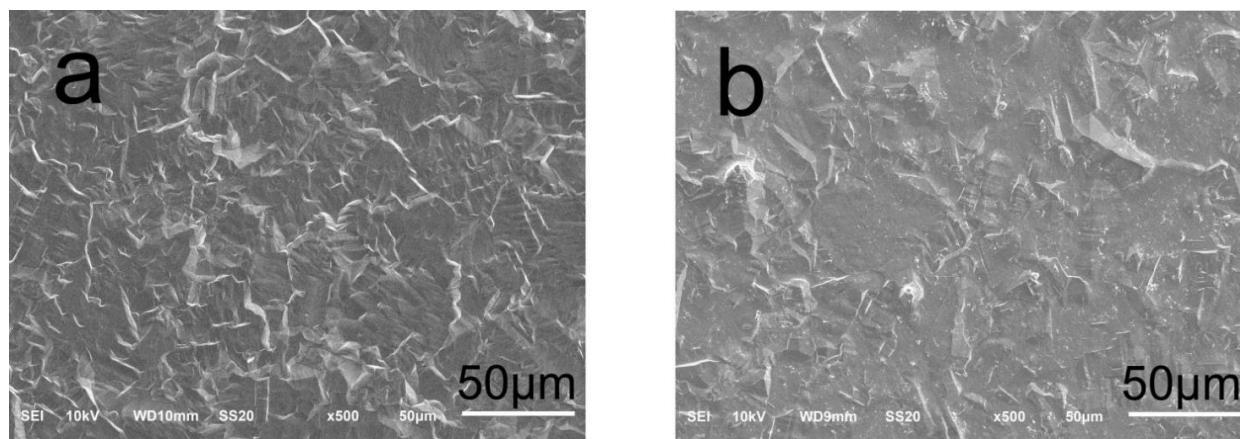


Figure 10. Surface morphologies of the electrode in 0.5 M HNO₃ + 2.0 mM Cl⁻ solutions polarized at 0.25 V for 100 s without (a) and with (b) MF.

To explain why MF increases the current in the prepassive region, a schematic plot is drawn (Figure 9). Without the application of MF (Figures 9a-9b), a large amount of Ni²⁺ ions accumulate around the electrode surface with the anodic dissolution of the nickel, and anions (NO₃⁻ and Cl⁻) in the bulk solution migrate to the electrode surface to satisfy the electric neutrality principle. When the concentration exceeds the solubility, the salt film (Figure 9b) is formed. This is verified by the experimental results shown in Figures 8c-8e, because the appearance of the blue area indicates that the

concentration of the corrosion products decreases. Under the protection of the salt film, the oxide film is easily formed on the electrode surface [49]. However, with the application of MF (Figures 9a'-9b'), F_L is induced to drive the ions away from the electrode surface (Figure 9a') so that the salt film is not easily formed. This is also supported by the experimental results shown in Figures 8c'-8e'. Without the protection of the salt film, it is too difficult to form the oxide film (Figure 9b'), resulting in the increase of the current in the prepassive region.

Figure 10 shows the surface morphologies of the Ni electrode potentiostatically polarized at 0.25 V for 100 s in 0.5 M $HNO_3 + 2.0\text{ mM } Cl^-$ solutions with and without MF. The electrode was corroded more seriously (Figure 10b) with the application of MF than that without the application of MF (Figure 10a), indicating the enhancement of the anodic dissolution by MF.

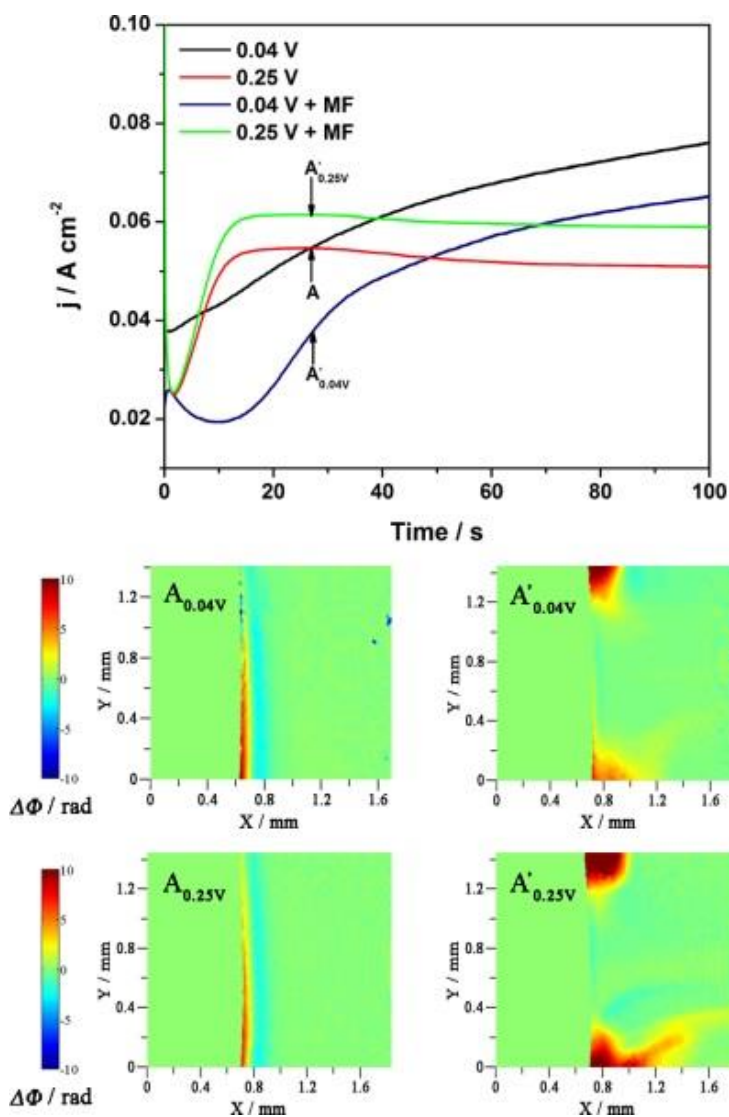


Figure 11. Top: the j - t curves of Ni in 0.5 M $HNO_3 + 2.0\text{ mM } Cl^-$ solutions at $E= 0.04\text{ V}$ and $E= 0.25\text{ V}$. Bottom: phase distributions at point A corresponding to Figure 10 (Top) without (A_{0.04V} and A_{0.25V}) and with MF (A'_{0.04V} and A'_{0.25V}).

The value of F_L is calculated as follows [50]:

$$F_L = j \times B \quad (1)$$

Both the intensity and the orientation of MF are kept constant in this study, and the value of F_L therefore depends on the current. Since the currents may vary at different potentials, the F_L values will be different. What will occur if the currents are the same at different potentials without the application of MF?

Figure 11(top) shows the j - t curves of Ni in 0.5 M HNO_3 + 2.0 mM Cl^- solutions at $E=0.04$ V and $E=0.25$ V without and with the application of MF, respectively. The two curves without MF intersect at point A, where the currents remain the same at different potentials. If the effects of MF are the same in different regions, the changes of the currents with MF should be the same, either increasing or decreasing. However, with the application of MF, the current decreases at $E=0.04$ V ($A'_{0.04V}$) but increases at $E=0.25$ V ($A'_{0.25V}$), which is in contrast to the relatively stable current without MF.

Figure 11(bottom) shows the phase distributions corresponding to point A without ($A_{0.04V}$ and $A_{0.25V}$) and with MF ($A'_{0.04V}$ and $A'_{0.25V}$). Under the same current (point A), without the application of MF, the surface concentration gradient of the corrosion products is more or less the same, and the phase distributions are therefore almost identical ($A_{0.04V}$ and $A_{0.25V}$). However, clear differences are observed here, with the gradient much lower in $A'_{0.04V}$ than in $A'_{0.25V}$, which can be attributed to the different rate-determining steps in different regions.

As mentioned above, in the active region, convection is induced by F_L to drive the anodic products (Ni^{2+}) and the active intermediate ions away from the surface of the electrode. The decrease of the concentration of the anodic products (Ni^{2+}) slightly affects the anodic processes because electron transfer is the rate-determining step. However, when the concentration of the active intermediate ions (such as $\text{Ni}(\text{ClH}^+)_{\text{ads}}$) decreases, the oxide film is formed easily on the surface of the electrode and the rate of reaction (3) decreases to inhibit the anodic processes. Thus, MF decreases the anodic current. In the prepassive region, the anodic current increases as the mass-transport processes (the rate-determining step) of the corrosion products (Ni^{2+}) are enhanced by MF due to the Lorentz-force-driven magnetohydrodynamic (MHD) effect [51-52].

Briefly, the concentration of the intermediate ions (such as $\text{Ni}(\text{ClH}^+)_{\text{ads}}$) plays a prominent role in the active region during the anodic dissolution of Ni, whereas the mass-transfer process of the anodic products (such as Ni^{2+}) dominates in the prepassive region. With the application of MF, the mass-transfer step is enhanced directly, while the electron-transfer step is affected indirectly.

4. CONCLUSIONS

In this study, in-line digital holography was used to observe the dynamic processes during the anodic dissolution of Ni in 0.5 M HNO_3 + 2.0 mM Cl^- with the application of a magnetic field.

The effects of MF are different in different regions. In the active region, MF is found to affect the electron-transfer step through enhancing the mass-transfer step. The convection of electrolytes induced by MF helps to drive away the intermediate ions, such as $\text{Ni}(\text{ClH}^+)_{\text{ads}}$ from the surface of the electrode, which can promote the active dissolution of nickel and inhibit the formation of the surface

film; thus, the active dissolution is checked by MF. In the prepassive region, mass transfer is the rate-determining step. The enhancement of the convection driven by F_L accelerates mass transfer so that MF increases the current.

ACKNOWLEDGEMENTS

This study was supported by the Chinese National Science Funds (No. 21473081, 51401094 and 21303077) and project funded by the Priority Academic Program Development of Jiangsu Higher Education Institutions.

Reference

1. N. Leventis, M.G. Chen, X.R. Gao, M. Canalias, P. Zhang, *J. Phys. Chem. B*, 102 (1998) 3512.
2. O. Devos, O. Aaboubi, J.P. Chopart, E. Merienne, A. Olivier, C. Gabrielli, B. Tribollet, *J. Phys. Chem. B*, 103 (1999) 496.
3. X.G. Yang, S.H. Chen, L. Li, C. Wang, *J. Electroanal. Chem.*, 586 (2006) 173.
4. S. Mühlenhoff, G. Mutschke, D. Koschichow, X. Yang, A. Bund, J. Fröhlich, S. Odenbach, K. Eckert, *Electrochim. Acta*, 69 (2012) 209.
5. S. Wang, Z.Y. Wang, J. Li, T. Zhang, *Int. J. Electrochem. Sci.*, 11 (2016) 1789.
6. E. Garcia-Ochoa, F. Corvo, J. Genesca, V. Sosa, P. Estupinan, *J. Mate. Eng. Perform.*, 26 (2017) 2129.
7. O. Devos, O. Aaboubi, J.P. Chopart, A. Olivier, *J. Phys. Chem. A*, 104 (2000) 1544.
8. S. Koehler, A. Bund, *J. Phys. Chem. B*, 110 (2006) 1485.
9. M.E.G. Lyons, R. O'Brien, M. Kinsella, C.M. Gloinn, G.P. Keeley, P.N. Scully, *Electrochem. Commun.*, 12 (2010) 1527.
10. T.K. Mahto, S. Chandra, C. Haldar, S.K. Sahu, *Rsc Advances*, 5 (2015) 47909.
11. A. Krause, M. Uhlemann, A. Gebert, L. Schultz, *Electrochim. Acta*, 49 (2004) 4127.
12. A. Bund, A. Ispas, *J. Electroanal. Chem.*, 575 (2005) 221.
13. J.A. Koza, M. Uhlemann, A. Gebert, L. Schultz, *Electrochim. Acta*, 53 (2008) 5344.
14. S. Mohan, G. Saravanan, A. Bund, *Electrochim. Acta*, 64 (2012) 94.
15. G. Galicia-Aguilar, G. Campo-Garcia, J.L. Ramirez-Reyes, A.L. Medina- Almazan, *Int. J. Electrochem. Sci.*, 12 (2017) 928.
16. O. Aaboubi, J.P. Chopart, J. Douglade, *J. Electrochem. Soc.*, 137 (1990) 1796.
17. R.A. Tacken, L.J.J. Janssen, *J. Appl. Electrochem.*, 25 (1995) 1.
18. N. Leventis, X. Gao, *Anal. Chem.*, 73 (2001) 3981.
19. G. Hinds, J.M.D. Coey, M.E.G. Lyons, *Electrochem. Commun.*, 3 (2001) 215.
20. Z.P. Lu, W. Yang, *Corros. Sci.*, 50 (2008) 510.
21. L. Li, W.J. Wang, C. Wang, S.H. Chen, *Electrochem. Commun.*, 11 (2009) 2109.
22. M. Kabasakaloglu, T. Kiyak, O. Sendil, A. Asan, *Appl. Surf. Sci.*, 193 (2002) 167.
23. J. Kunze, V. Maurice, L.H. Klein, H.H. Strehblow, P. Marcus, *Electrochim. Acta*, 48 (2003) 1157.
24. L. Li, C. Wang, B.Y. Yuan, S.H. Chen, *Electrochem. Commun.*, 10 (2008) 103.
25. B.Y. Yuan, S.H. Chen, X.G. Yang, C. Wang, L. Li, *Electrochem. Commun.*, 10 (2008) 392.
26. A. Anand, V.K. Chhaniwal, C.S. Narayanamurthy, *Appl. Opt.*, 45(2006) 904.
27. Z.P. Lu, D.L. Huang, W. Yang, J. Congleton, *Corros. Sci.*, 45 (2003) 2233.
28. Q.K. Yu, Y. Miyakita, S. Nakabayashi, R. Baba, *Electrochem. Commun.*, 5 (2003) 321.
29. C. Wang, S.H. Chen, X.G. Yang, L. Li, *Electrochem. Commun.*, 6 (2004) 1009.
30. X.G. Yang, S.H. Chen, C. Wang, L. Li, *J. Serb. Chem. Soc.*, 71 (2006) 67.
31. Z.P. Lu, C.B. Huang, D.L. Huang, W. Yang, *Corros. Sci.*, 48 (2006) 3049.

32. R. Sueptitz, K. Tschulik, M. Uhlemann, A. Gebert, L. Schultz, *Electrochim. Acta*, 55 (2010) 5200.
33. R. Sueptitz, K. Tschulik, M. Uhlemann, L. Schultz, A. Gebert, *Electrochim. Acta*, 56 (2011) 5866.
34. F.M.F. Rhen, J.M.D. Coey, *J. Phys. Chem. B*, 110 (2006) 6274.
35. B.Y. Yuan, C. Wang, L. Li, S.H. Chen, *Electrochem. Commun.*, 11 (2009) 1373.
36. J. Hu, C.F. Dong, X.G. Li, K. Xiao, *J. Mater. Sci. Technol.*, 26 (2010) 355.
37. B.Y. Yuan, C. Wang, L. Li, S.H. Chen, *Corros. Sci.*, 58 (2012) 69.
38. G.F. Gao, B.Y. Yuan, C. Wang, L. Li, S.H. Chen, *Int. J. Electrochem. Sci.*, 9 (2014) 2565.
39. Y. Oshikiri, R. Aogaki, M. Miura, A. Sugiyama, R. Morimoto, M. Miura, I. Mogi, Y. Yamauchi, *Electrochem.*, 83 (2015) 549.
40. X.P. Wang, J.J. Zhao, Y.P. Hu, L. Li, C. Wang, *Electrochim. Acta*, 117 (2014) 113.
41. X.G. Yang, S.H. Chen, C. Wang, L. Li, *Electrochem. Commun.*, 6 (2004) 643.
42. R. Sueptitz, J. Koza, M. Uhlemann, A. Gebert, L. Schultz, *Electrochim. Acta*, 54 (2009) 2229.
43. C. Wang, S.H. Chen, X.L. Yu, *J. Electrochem. Soc.*, 143 (1996) L283.
44. C. Wang, S.H. Chen, H.Y. Ma, *J. Electrochem. Soc.*, 145 (1998) 2214.
45. Z.P. Lu, T. Shoji, W. Yang, *Corros. Sci.*, 52 (2010) 2680.
46. Y.C. Tang, A.J. Davenport, *J. Electrochem. Soc.*, 154 (2007) C362.
47. E.E. Abd El Aal, W. Zakria, A. Diab, S.M. Abd El Haleem, *J. Mate. Eng. Perform.*, 12 (2003) 172.
48. N.A. Darwish, F. Hilbert, W.J. Lorenz, H. Rosswag, *Electrochim. Acta*, 18 (1973) 421.
49. B.Y. Yuan, J.L. Zhang, G.F. Gao, L. Li, C. Wang, *Electrochem. Commun.*, 27 (2013) 116.
50. O.Y. Gorobets, V.Y. Gorobets, D.O. Dercha, O.M. Brukva, *J. Phys.Chem.C*, 112 (2008) 3373.
51. R. Sueptitz, J. Koza, M. Uhlemann, A. Gebert, L. Schultz, *Electrochim. Acta*, 54 (2009) 2229.
52. T. Weier, K. Eckert, S. Mühlenhoff, C. Cierpka, A. Bund, M. Uhlemann, *Electrochem. Commun.*, 9 (2007) 2479.

© 2018 The Authors. Published by ESG (www.electrochemsci.org). This article is an open access article distributed under the terms and conditions of the Creative Commons Attribution license (<http://creativecommons.org/licenses/by/4.0/>).